Antiviral Research 178 (2020) 104806

Contents lists available at ScienceDirect

Antiviral Research

journal homepage: www.elsevier.com/locate/antiviral

Research paper

Antiviral efficacy against influenza virus and pharmacokinetic analysis of a novel MEK-inhibitor, ATR-002, in cell culture and in the mouse model

Martin Laure[a,b], Hazem Hamza[a,b,c], Julia Koch-Heier[a,b], Martin Quernheim[d], Christin Müller[e], Andre Schreiber[f], Gerhard Müller[g], Stephan Pleschka[e], Stephan Ludwig[f], Oliver Planz[a,b,*]

[a] Interfaculty Institute for Cell Biology, Department of Immunology, Eberhard Karls University, Tübingen, Germany
[b] Atriva Therapeutics GmbH, Christophstr. 32, 72072, Tübingen, Germany
[c] Virology Laboratory, Environmental Research Division, National Research Centre, Cairo, Egypt
[d] Chemcon GmbH, Engesserstr. 4B, 79108, Freiburg I. Brsg., Germany
[e] Institute of Medical Virology, Justus Liebig University, Giessen, Germany
[f] Institute of Virology, Westfaelische Wilhelms-University, Muenster, Germany
[g] Gotham Therapeutics, New York, USA

ARTICLE INFO

Keywords:
Influenza virus
MEK-Inhibitor
Pharmacokinetic
Bioavailability
Antiviral

ABSTRACT

Antiviral therapies against influenza are required, especially for high-risk patients, severe influenza and in case of highly pathogenic influenza virus (IV) strains. However, currently, licensed drugs that target the virus directly are not very effective and often lead to the development of resistant IV variants. This may be overcome by targeting host cell factors that are required for IV propagation. IV induces a variety of host cell signaling cascades, such as the Raf/MEK/ERK kinase pathway. The activation of this pathway is necessary for IV propagation. MEK-inhibitors block the activation of the pathway on the bottleneck of the signaling cascade leading to impaired virus propagation. In the present study, we aimed to compare the antiviral potency and bioavailability of the MEK-inhibitor CI-1040 versus its major active metabolite ATR-002, *in vitro* as well as in the mouse model. In cell culture assays, an approximately 10-fold higher concentration of ATR-002 is required to generate the same antiviral activity as for CI-1040. Interestingly, we observed that considerably lower concentrations of ATR-002 were required to achieve a reduction of the viral load *in vivo*. Pharmacokinetic studies with ATR-002 and CI-1040 in mice have found the C_{max} and AUC to be far higher for ATR-002 than for CI-1040. Our results thereby demonstrate the *in vivo* superiority of the active metabolite ATR-002 over CI-1040 as an antiviral agent despite its weaker cell membrane permeability. Therefore, ATR-002 is an attractive candidate for development as an efficient antiviral agent, especially given the fact that a treatment based on cellular pathway inhibition would be far less likely to lead to viral drug resistance.

1. Introduction

Despite intensive efforts to fight and prevent influenza, it still remains a worldwide threat. Seasonal outbreaks are estimated to cause 290,000–650,000 deaths among adults, and over 100,000 deaths among children under the age of 5 years old, annually (Iuliano et al., 2018). Hospitalization rates range between 3 and 5 million per year (Lambert and Fauci, 2010), and damage to national economies is considerable (Putri et al., 2018; Tempia et al., 2019). Vaccination strategies are the core of influenza management (Belshe et al., 2007; Nichol et al., 1995; Nichol and Treanor, 2006; Radin et al., 2016), but reliable and effective drugs for immediate treatment once the disease has manifested are equally important. However, for both the well-known and direct acting classes of antivirals available for clinical use [neuraminidase inhibitors (e.g. oseltamivir, zanamivir, peramivir) and M2 ion-channel inhibitors (e.g. amantadine, rimantadine)], resistance is increasingly reported (Baranovich et al., 2010; Correia et al., 2015; Dong et al., 2015; Kiso et al., 2004). Even against the recently developed novel anti influenza drug Baloxavir, an inhibitor of the cap-dependent endonuclease activity within the polymerase subunit PA of influenza A and B viruses, resistance is already occurring at a frightening frequency (Omoto et al., 2018). For example, insensitive mutant strains which have the same fitness as wild type strains have been reported, as well as events of human to human transmission of resistant

* Corresponding author. Eberhard Karls University Tübingen Interfaculty, Institute for Cell Biology, Department of Immunology, Auf der Morgenstelle 15, 72076, Tübingen, Germany.
E-mail address: oliver.planz@uni-tuebingen.de (O. Planz).

https://doi.org/10.1016/j.antiviral.2020.104806
Received 30 October 2019; Received in revised form 10 April 2020; Accepted 13 April 2020
Available online 15 April 2020
0166-3542/ © 2020 The Authors. Published by Elsevier B.V. This is an open access article under the CC BY license (http://creativecommons.org/licenses/BY/4.0/).

variants. This emphasizes the inherent potential of the influenza virus (IV) to adapt quickly when targeted directly and thereby to escape current treatment options.

An alternative approach to prevent drug resistance is to target essential cellular pathways on which the virus depends for survival. We were able to demonstrate that the MEK-inhibitor CI-1040, a small-molecule inhibitor of the dual-specificity kinases MEK (mitogen-activated protein kinase kinase) −1 and MEK2, that was previously used in clinical studies against cancer (Lorusso et al., 2005; Sebolt-Leopold, 2004) showed a strong antiviral activity against IV *in vitro* and *in vivo* (Droebner et al., 2011; Haasbach et al., 2017). Infection with IV leads to a bi-phasic activation of the Raf/MEK/ERK signaling pathway and it seems that the late stage of activation is the functionally most relevant. In this phase of the replication cycle the IV needs to drive export of the viral genome-containing ribonucleoprotein (vRNP)-complexes out of the nucleus and into the cytoplasm. Accordingly, inhibition of the pathway using MEK-inhibitors results in impaired virus propagation concomitant with nuclear retention of vRNPs in the nucleus (Droebner et al., 2011; Haasbach et al., 2017; Ludwig et al., 2006; Planz, 2013; Pleschka et al., 2001). Moreover, activation of the Raf/MEK/ERK pathway is required by the virus for phosphorylation of viral proteins and constant activation strongly supports virus propagation (Olschlager et al., 2004; Pleschka et al., 2001).

A phase I study reported that maximum CI-1040 plasma concentrations (C_{max}) and the area under the curve (AUC) of the plasma concentration are insignificant, even when high doses of CI-1040 were administered and development was therefore abandoned (Lorusso et al., 2005). Interestingly, the same study also observed approximately 5-fold higher plasma concentrations for the active metabolite of CI-1040, PD-0184264 (now designated ATR-002). However, due to its acid group, which is thought to obstruct the ability of a molecule to penetrate cellular membranes, pharmaceutical development of PD-0184264 was not pursued further even though the 50% inhibitory concentration (IC_{50}) value of PD-0184264 for MEK inhibition was slightly lower (5.73 nM) when compared to CI-1040 (17.00 nM) (Sebolt-Leopold et al., 1999; Tecle et al., 2009). Consequently, we were interested to investigate whether this active metabolite would also have antiviral potency against IV.

Here, we demonstrate the *in vitro* and *in vivo* antiviral potential of the MEK-inhibitor PD0184264 (ATR-002, the active metabolite of CI-1040) against IVs. Moreover, we have elucidated the antiviral mode of action against both influenza A and B viruses.

2. Materials and methods

2.1. Drugs

CI-1040 [2-(2-chloro-4-iodophenylamino)-N-(cyclopropylmethoxy)-3,4-difluoro benzamide], (M = 478,66 g/mol) and ATR-002 (PD0184264) [2-(2-chloro-4-iodophenylamino)-N-3,4-difluoro benzoic acid], (M = 409,55 g/mol) were synthesized at ChemCon GmbH (Freiburg, Germany). For all cell culture experiments, fresh 10 mM stock solutions of CI-1040 and ATR-002 were prepared in DMSO (Merck-Millipore, Darmstadt, Germany) and further diluted in the respective media or buffer.

Synthesis of CI-1040 was achieved by the coupling of o-cyclopropylmethylhydroxylamin hydrochlorid and ATR-002 (Fig. 1), which were prepared by two synthetic routes. The amide bond was formed using 1-propanephosphonic anhydride (T3P) to activate the carboxylic acid. The side chain o-cyclopropylmethylhydroxylamin hydrochlorid was prepared in a one-pot reaction starting from ethyl-N-acetohydroxyacetamidate. The active substance ATR-002 was prepared in one step by a nucleophilic aromatic substitution. Next, 2,3,4 Trifluorobenzoic acid and 2-chloro-4-iodo aniline were coupled using lithium amide as an efficient base in THF/acetonitrile.

2.2. Cells and viruses

Human adenocarcinoma type II alveolar lung epithelial cells (A549, ATCC® CCL185™) and Madin-Darby canine kidney cells (MDCK II, ATCC® CRL2936™) were purchased from ATCC and cultured in Iscove's Modified Dulbecco's Medium (IMDM, Thermo Fisher Scientific, Waltham, Massachusetts, USA) supplemented with 10% (v/v) fetal bovine serum (FBS, Sigma-Aldrich, St. Louis, Missouri, U.S.A.), 100 U/mL penicillin, and 100 µg/mL streptomycin (Sigma-Aldrich, St. Louis, Missouri, U.S.A.). Cells were maintained in a 37 °C and 5% CO_2 atmosphere. Human PBMCs were provided by healthy donors and purified by standard Ficoll gradient.

Virus inhibition experiments were carried out with influenza A virus (IAV) strain RB1 [A/Regensburg/D6/09 (H1N1pdm09)] with a multiplicity of infection (MOI) of 0.001, IV A/Fukui/20/2004 (H3N2) with a MOI of 0.001 and influenza B virus (IBV) strain B/Lee/40 with a MOI of 0.001 and B/Münster/341-200/18 with a MOI of 5.

2.3. Mice

Eight-week-old male NMRI mice (Charles River Laboratories, Germany) with a body weight of 23.9–36.5 gr. at administration were used for pharmacokinetic studies. Eight-week-old female C57BL/6 mice (Charles River Laboratories, Germany) with a body weight of 21.0–24.0 gr. at administration were used for the antiviral studies. The animals were fed with standard food. Drinking water was available *ad libitum*.

2.4. Drug administration to mice

Drugs were either administered using a single dosing on test day 1 by oral gavage or by intravenous (i.v.) bolus injection into a tail vein. The injection speed was 15 s/dose with an administration volume of 200 µl.

2.5. Progeny virus inhibition assay

A549 cells were inoculated with the aforementioned IAV strains at the respective MOI prepared in phosphate buffered saline (PBS) supplemented with 0.2% (w/v) bovine serum albumin (BSA, Carl Roth, Karlsruhe, Germany), 1 mM $MgCl_2$, 0.5 mM $CaCl_2$, 100 U/mL penicillin, 100 µg/mL streptomycin (Merck, Germany) for 45 min at 37 °C and 5% CO_2. Inocula were removed, cells were rinsed with PBS, and supplemented with 1 mL IV infection media (Dulbecco's Modified Eagle Medium; DMEM; Thermo Fisher Scientific, Waltham, Massachusetts, U.S.A supplemented with 0.2% BSA, 1 mM $MgCl_2$, 0.5 mM $CaCl_2$, 100 U/mL penicillin, 100 µg/mL streptomycin, and 2 µg/mL TPCK-treated Trypsin, containing different concentrations of either CI-1040 or ATR-002 (100 µM, 50 µM, 10 µM, 5 µM, 1 µM, 0.5 µM, and 0.1 µM, final DMSO concentration 1% for 24 h at 37 °C in 5% CO_2).

2.6. Influenza virus titration (AVICEL® plaque assays)

All AVICEL® plaque assays were carried out as previously described (Haasbach et al., 2011; Matrosovich et al., 2006). Briefly, MDCK-II virus-infected cells were immunostained 22 h post infection (hpi) with mouse anti-IAV nucleoprotein monoclonal antibody (Bio-Rad, Hercules, California, USA) followed by peroxidase-labelled anti-mouse antibody and True Blue™ peroxidase substrate (SeraCare, Life Sciences, Milford, Massachusetts U.S.A.).

2.7. Determination of viral load in lungs

Mice were sacrificed by CO_2 gassing. Lungs were removed, weighed and transferred into a Lysing Matrix D tube (MP Biomedicals, Eschwege, Germany). Next, 500 µl ice-cold PBS was added and the tissue organs were shredded using the FastPrep FP 120 (Savant). The

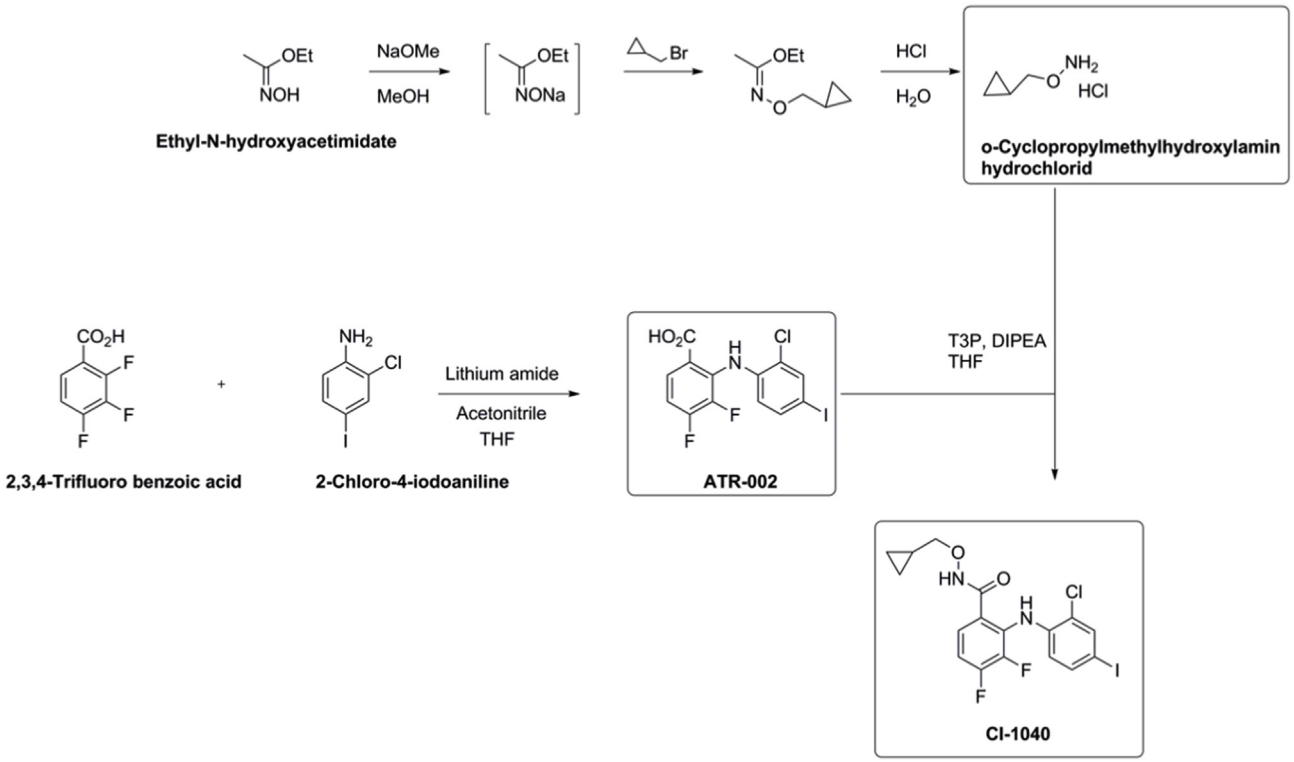

Fig. 1. Synthesis of ATR-002 and CI-1040. The side chain o-cyclopropylmethylhydroxylamin hydrochlorid was prepared in a one pot reaction starting from ethyl-N-acetohydroxacetamidate. ATR-002 was prepared in a one step by nucleophilic aromatic substitution. 2,3,4 Triflourobenzoic acid and 2-chloro-4-iodo aniline were coupled by using lithium amide as an efficient base in THF/acetonitrile. The synthesis of CI-1040 was achieved by coupling of the two building blocks o-cyclopropylmethylhydroxylamin hydrochlorid and ATR-002. The amide bond was formed using 1-propanephosphonic anhydride (T3P) to activate the carboxylic acid of ATR-002.

homogenized tissue was centrifuged for 10 min at 18,000 × *g* at 4 °C. Supernatant was transferred into sterile 1.5 mL safe-lock tubes (Eppendorf, Hamburg, Germany) and kept on ice until further storage at −80 °C. To determine the virus load, supernatant was thawed on ice and an AVICEL® plaque assay using MDCK II cells was performed.

2.8. Cell viability assay (WST-Assay)

A549 cells, MDCK cells and human PBMCs were seeded in a 96-well flat-bottom tissue plate (Greiner, Bio-One, Frickenhausen, Germany) and were grown over-night as described in section 2.2. Thereafter, cells were treated with different concentrations of ATR-002 (100 µM, 50 µM, 10 µM, 5 µM, 1 µM, 0.5 µM, and 0.1 µM) dissolved in 100 µl IMDM supplemented with 5% FBS with a final DMSO concentration of 1% (v/v). Cells were cultured at 37 °C with 5% CO_2 for 24 h. Thereafter, 10 µl WST-1 reagent (Roche, Basel, Switzerland) was added to the culture medium and incubated for 4 h. Thereafter, the formazan dye formed was quantified on an ELISA plate reader (Molecular Devices, San Jose, California, U.S.A.) at 405 nm.

2.9. Immunofluorescence staining and microscopy

For immunofluorescence analysis of infected and inhibitor-treated A549 cells, samples were washed with PBS and fixed with ice cold methanol (−20 °C, Carl Roth, Karlsruhe, Germany) for 10 min at 4 °C. Afterwards cells were washed with PBS and blocked with 3% (w/v) BSA in PBS for 1 h at 21 °C (room temperature). Primary antibodies against influenza B virus (IBV) NP (Bio-Rad, Hercules, California, USA) and IBV-M1 (GeneTex) were diluted 1:1000 in 3% BSA in PBS (BSA/PBS). Primary antibody incubation was performed for 1 h at RT. After washing with BSA/PBS, samples were incubated for 45 min in BSA/PBS containing 1:800 diluted anti-mouse Alexa 488 IgY (Thermo Fisher Scientific, Waltham, Massachusetts, U.S.A) and anti-rabbit Alexa 561 IgG (Thermo Fisher Scientific, Waltham, Massachusetts, U.S.A) secondary antibodies and DAPI (5 mg/mL) (4′,6-diamino-2-phenylindole, Thermo Fisher Scientific, Waltham, Massachusetts, U.S.A) diluted 1:10000. After the final PBS wash, samples were mounted onto object slides with Fluorescence Mounting Medium (Dako, Jena, Germany). Immunofluorescence analysis was performed with an epifluorescence microscope (Axiovert 200M, Carl Zeiss, Jena Germany).

2.10. Determination of IC_{50} values for CI-1040 and ATR-002

Detailed methods for the cell free kinase assay and the kinase assays in A549, MDCK cells and human PBMCs were described in the supplementary (Supplementary S1).

2.11. Western blot analysis

Protein concentration was determined by BCA Protein Assay (Thermo Fisher Scientific, Waltham, Massachusetts, U.S.A.) before the lysates were subjected to sodium dodecyl sulphate-polyacrylamide gel electrophoresis (SDS-PAGE) and transferred onto polyvinylidene fluoride (PVDF) membranes (Bio-Rad, Hercules, California, U.S.A.). Membranes were incubated with a phospho-specific anti pERK mAb (1:500; Santa Cruz, Biotechnology, Dallas, Texas, U.S.A.) diluted in 5% BSA/TBS/T (20 mM Tris–HCl pH 7.6, 140 mM NaCl, 0.05% Tween 20) overnight at 4 °C. After stripping (Merck Millipore, Darmstadt, Germany) bound antibodies and washing in TBS/Tween buffer, total ERK2 was detected using anti-ERK2 mAb (1:500; Santa Cruz, Biotechnology, Dallas, Texas, U.S.A.) for 1 h at RT followed by incubation with a peroxidase-coupled, species-specific HRP-conjugated anti-mouse monoclonal secondary antibodies (1:800; Santa Cruz, Biotechnology, Dallas, Texas, U.S.A.) and a standard enhanced

chemiluminescence reaction (Santa Cruz, Biotechnology, Dallas, Texas, U.S.A.). Specific bands were quantified on the Fusion software.

2.12. Determination of pERK/ERK2 ratio by Wes™ analysis

Wes™ capillary electrophoresis by ProteinSimple® was used to identify and quantify pERK/ERK2. Cell lysates were diluted 1:2 with 0.1X Sample Buffer (ProteinSimple, Abingdon, Oxford, UK) and analyzed using specific antibodies. The primary antibodies pERK mouse monoclonal IgG2a and ERK-2 mouse monoclonal IgG2a were purchased from Santa Cruz Biotechnology (Santa Cruz Biotechnology, Dallas, Texas, U.S.A.) and used at 1:25 dilutions in antibody diluent (Protein Simple, Abingdon, Oxford, UK). The anti-rabbit secondary antibody and all used reagents were also purchased from ProteinSimple and were ready to use.

2.13. Preparation of compounds for pharmacokinetic analysis

For i.v. administration, 30.65 mg CI-1040 was dissolved in 0.075 mL DMSO (Sigma-Aldrich, St. Louis, Missouri, U.S.A.) and further diluted with 0.225 mL Cremophor EL (Merck-Millipore, Darmstadt, Germany) and 2.7 mL PBS (Thermo Fisher Scientific, Waltham, Massachusetts, U.S.A.). Next, 34.88 mg ATR-002 was dissolved in 0.075 mL DMSO and further diluted with 0.225 mL Cremophor EL and 2.7 mL PBS. For oral administration 202.5 mg CI-1040 was dissolved in 0.5 mL DMSO, 1.5 mL Cremophor EL, and 8.0 mL PBS. Accordingly, 81.0 mg ATR-002 was dissolved in 0.2 mL DMSO, 0.6 mL Cremophor EL, and 3.2 mL PBS.

2.14. Blood sampling and preparation of plasma

Experiments were performed at LPT GmbH (Hamburg, Germany). Whole blood from mice, taken under isoflurane anesthesia, was collected to obtain at least 2 × 100 µL Li-Heparin plasma of 3 animals per group and time-points at the following times: 0 (predose), 15 min, 30 min, 1 h, 2 h, 4 h, 6 h, 8 h, and 24 h (test day 2) after administration. The whole blood samples were instantly cooled using an Iso-Therm-Rack system (Eppendorf AG, Hamburg, Germany) until centrifugation within 0.5 h after withdrawal. Immediately after centrifugation, the samples were stored at −20 °C until further analysis. Plasma analysis was performed using standard procedures at Prolytic GmbH (Frankfurt, Germany).

2.15. Preparation of compounds to investigate virus titer reduction in the lungs of mice

For oral application of 25 mg ATR-002/kg bodyweight, 10 mg of ATR-002 was dissolved in 50 µl DMSO (Sigma-Aldrich, St. Louis, Missouri, U.S.A.) and further diluted with 0.15 mL Cremophor EL and 0.8 mL PBS. For application of 8.4 mg/kg and 2.8 mg/kg, 3.36 mg or 1.12 mg ATR-002 was dissolved in 50 µl DMSO and further diluted with 0.15 mL Cremophor EL and 0.8 mL PBS. Additionally, 202.5 mg CI-1040 was dissolved in 0.5 mL DMSO, 0.15 mL Cremophor EL, and 0.8 mL PBS.

2.16. Treatment and preparation of MDCK cells for detection of intracellular deposition

MDCK-II cells were seeded in 3.5 cm dishes of 6-well plates (Greiner, Bio-One, Frickenhausen, Germany) and grown in DMEM supplemented with 10% FBS and 100 U/ml Penicillin and 100U/mL Streptomycin. After washing the cells were incubated with DMEM/BA (DMEM containing 0.2% BA, P/S), which either contained CI-1040 or ATR-002 at a concentration of 10 or 50 µM solved in DMSO, or just DMSO (negative control). At 0.5, 2 and 6 h post inhibitor/DMSO-treatment cells (infected or uninfected) were washed with PBS^{++} scraped off, collected in 15 mL tube and pelleted by centrifugation. The supernatant (SN) was removed and the cells were resuspended in 10 mL PBS^{++} for washing. After pelleting the SN was removed and the cells transferred into a 1.5 mL reaction tube in 1 mL PBS^{++}. After precipitation and removal of the SN the cell pellet was dissolved in 50 µl of 6 M Guanidiniumthiocyanate (Sigma-Aldrich, St. Louis, Missouri, U.S.A.) and stored at −70 °C for further processing. All experiments were performed in triplicate. Lysed cells were used to determine intracellular deposition of either CI-1040 or ATR-002 with mass spectrometry using the standard procedures at Prolytic GmbH (Frankfurt, Germany).

3. Results

3.1. Synthetic scheme for the synthesis of ATR-002 and CI-1040

One initial aim of the work presented here was the development of an efficient route towards synthesis of CI-1040. The synthesis was achieved by the coupling of the two building blocks o-cyclopropylmethylhydroxylamin hydrochlorid and 2-(2-Chloro-4-iodo-phenylamino)-3,4-difluoro benzoic acid (ATR-002), which were prepared by two separate synthetic routes. ATR-002 was prepared in a one-step reaction with 2,3,4 Triflourobenzoic acid and 2-Chloro-4-iodo aniline by nucleophilic aromatic substitution (Fig. 1). The synthesis of o-cyclopropylmethylhydroxylamin hydrochlorid is described in the Materials and methods section.

3.2. Modeling of CI-1040 and ATR-002 onto MEK

Based on a thorough visual inspection of the X-ray structure (Protein Data Bank; 1s9j.pdb) of a ternary complex of MEK-1, ATP and a small-molecule inhibitor structurally closely related to ATR-002 and CI-1040 (Ohren et al., 2004), we modified the inhibitor structure to resemble ATR-002 in order to rationalize the binding mode. Energetic relaxation resulted in a model structure in which ATR-002 is docked into the type-III inhibitor-binding pocket of MEK-1 (Fig. 2A). As exemplified in the interaction diagram (Fig. 2B), the B-ring is perfectly accommodated in its original binding pocket delineated by predominately hydrophobic residues. The Iodine atom is within a 3.7 Å of the Val-127 backbone carbonyl oxygen atom. The A-ring remains very close to its original position within the parent complex structure. The side chain of Lys-97 slightly changes its position towards the charged carboxylate of ATR-002 and together with the gatekeeper residue Met-143 it physically sequesters the type-III inhibitor pocket from the active site of the enzyme in which ATP is concurrently bound. Given the close structural resemblance of ATR-002 to the first-generation MEK1/2 inhibitors, we strongly believe that the binding mode exemplified in this molecular modeling study reflects the physiologically relevant situation.

3.3. Antiviral activity of ATR-002 against influenza virus

The antiviral activity of ATR-002 against IAV was investigated in a standard virus inhibition assay (Fig. 3). We demonstrated a reduction in viral titers of the pandemic H1N1 strain A/Regensburg/D6/2009 (RB1, H1N1pdm09) after treatment with 100 µM or 50 µM ATR-002, respectively (Fig. 3A). Moreover, a quite similar pattern of titer reduction was observed for the seasonal H3N2 strain A/Fukui/20/2004 (H3N2) strain, with the two above-mentioned ATR-002 concentrations. Comparing the effect of ATR-002 on these two viruses, 10 µM ATR-002 resulted in a titer reduction of roughly 50% of H1N1pdm09, a stronger decrease was found for the H3N2 strain (87%). Moreover, 1 µM ATR-002 was insufficient to significantly affect virus titers of both, the H1N1pdm09 and the H3N2 strains (Fig. 3A, D). Thus, in comparison to the virus reduction observed with 10 µM CI-1040 (Haasbach et al., 2017) an almost 10-fold higher concentration of ATR-002 is needed to achieve similar reduction of progeny virus.

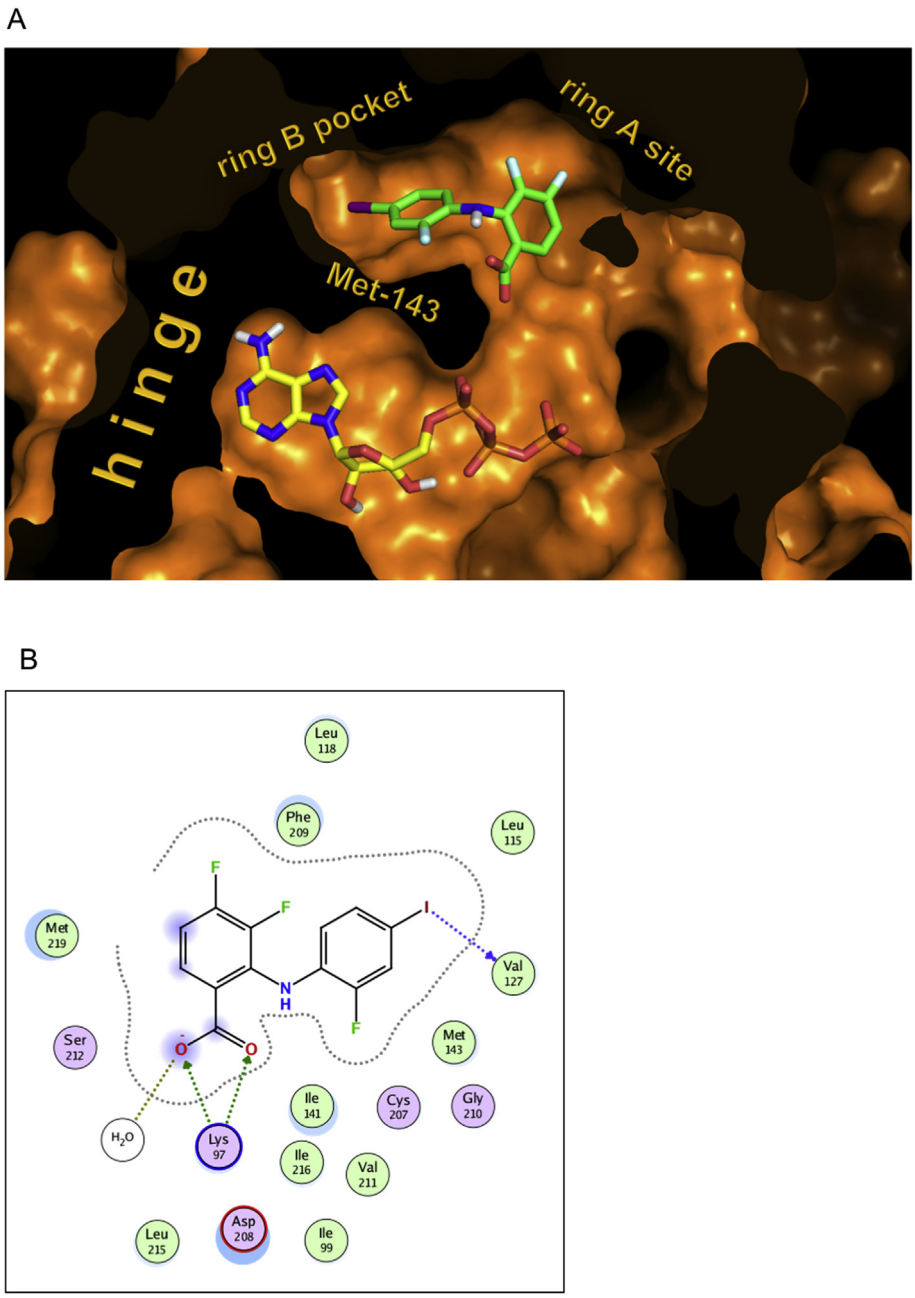

Fig. 2. Modelling of ATR-002 into the MEK binding region. (A) View into the active site of the modelled MEK-1 inhibitor complex structure obtained from the Protein Data Bank (1s9j.pdb). The protein is shown in a solvent-accessible surface representation, while the ATP and inhibitor molecule are depicted in stick mode. The hinge region is shown on the left. **(B)** Schematic interaction diagram of ATR-002 bound to MEK-1. The halogen bond of the iodine atom in ring-B to Val-127 is shown explicitly.

As an important step towards developing an effective antiviral drug, the pharmacological parameters, both the half maximal effective concentration (EC_{50}) and the 50% cytotoxic concentration (CC_{50}) were determined. The CC_{50} value for ATR-002 was 271.8 μM on A549 cells and 188.6 μM on MDCK II cells (Fig. 3C, H). Afterwards, the EC_{50}, was analyzed using a wide range of ATR-002 concentrations on A549 cells infected with either the H1N1pdm09 or the H3N2 strain and on MDCK II cells infected with B/Lee/40. EC_{50} values for ATR-002 against these three viruses were in the same range (4.190–6.356 μM) (Fig. 3B, E, G). Comparison of the CC_{50} and EC_{50} of ATR-002 resulted in a selectivity index (SI) of 42.8 for H1N1pdm09, 60.4 for H3N2, and 45.0 for B/Lee/40.

On a molecular level, the antiviral action of MEK-inhibitors was shown to be due to a nuclear retention of viral vRNPs (Pleschka et al., 2001). However, while MEK-inhibitors such as U0126 (Ludwig et al., 2004) and CI-1040 (Haasbach et al., 2017) also impair IBV replication, it had not yet been shown whether this also occurs via the same mechanism. While vRNPs of B/Münster/341-200/18 are readily translocated to the cytoplasm shown by a predominant cytoplasmic staining of NP 12 hpi (Fig. 4, upper lane), all tested concentrations of both, CI-1040 (Fig. 4, middle lane) and ATR-002 (Fig. 4, lower lane) blocked the export of newly synthesized vRNPs as indicated by the prevalent staining of NP in the nuclei.

3.4. Determination of IC_{50} kinase inhibition values for CI-1040 and ATR-002

The 10-fold higher concentrations of ATR-002 needed to achieve the

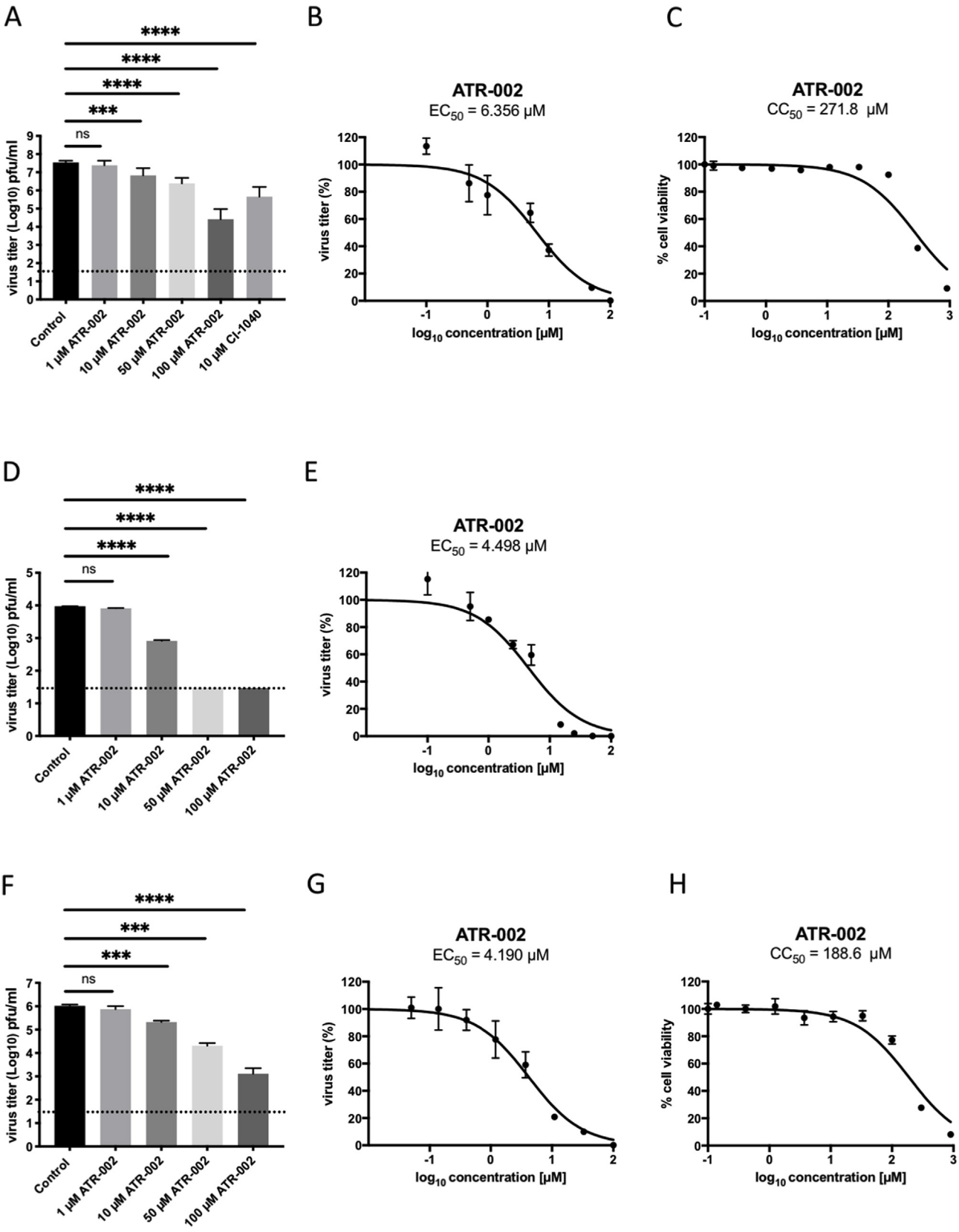

(caption on next page)

same antiviral effect as of CI-1040 is striking, given the fact that similar IC_{50} values towards MEK (CI-1040: 17.0 nM; ATR-002: 5.7 nM) were published for these two compounds (Sebolt-Leopold et al., 1999; Tecle et al., 2009). Therefore, we re-determined the IC_{50} values for CI-1040 and ATR-002 in a cell free environment (Fig. 5A, B), in two different cell lines (A549; Fig. 5C and MDCK; Fig. 5D), and in human PBMCs (Fig. 5E).

The IC_{50} of the MEK-Inhibitors CI-1040 and its acid metabolite ATR-

Fig. 3. Antiviral activity of ATR-002 against IV H1N1pdm09, H3N2, and nuclear vRNP-retention of IBV after pathway inhibition. (A) A549 were infected with RBI (MOI = 0.001) to determine virus titer reduction. Dose dependent inhibition was found for ATR-002 compared to solvent control. 100 μM ATR-002 resulted in a 99.87% ± 0.01% reduction of virus titer (Unpaired *t*-test with Welch's correction $P > 0.0001$). Similar significance was found using 50 μM ATR-002 (Unpaired *t*-test with Welch's correction $P > 0.0001$) while no significant virus titer reduction was found using 10 μM and 1 μM ATR-002.10 μM CI-1040 also resulted in a strong reduction of virus titer (Unpaired *t*-test with Welch's correction $P > 0.0001$). The figure represents the results of three experiments. **(B)** A549 cells were infected with RBI (MOI = 0.001) and treated with different concentrations of ATR-002 to determine the EC_{50} value. The data shown here is an average of four independent experiments. A549 cells **(C)** and MDCK II cells **(H)** were treated with different concentrations of ATR-002 for 24 h followed by 4 h WST-staining to determine the CC_{50} values. **(D)** The potency of ATR-002 against H3N2 after 24 h (p.i) was tested. Linear regression analysis in order to calculate the EC_{50} of ATR-002 against H3N2 **(E)** and against B/Lee/40 **(G)**. data shown in $\log_{10}$ concentration. All statistical tests were performed using GraphPad Prism 8. **(F)** Antiviral potential of ATR-002 against B/Lee/40. All antiviral data was analyzed using an Unpaired *t*-test with Welch's correction. Asterisks above bars represent statistical significance.

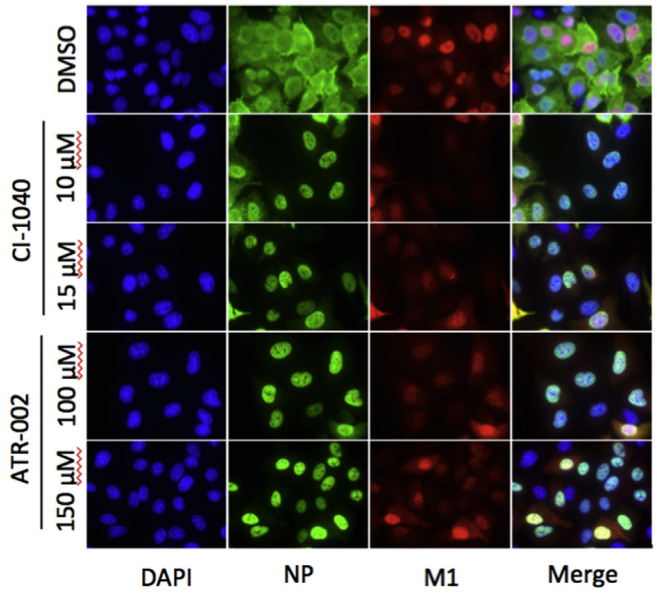

Fig. 4. Nuclear vRNP-retention of IBV after pathway inhibition.
Human lung epithelial cells (A549) were infected with Influenza B/Münster/341-200/18 at a multiplicity of infection (MOI) of 5 for 30 min at 33 °C. Cells were prepared for immunofluorescence staining of the viral nucleoprotein (NP) (green) and matrix protein 1 (M1) (red). Anti-NP (Bio-Rad) and anti-M1 (GeneTex) were used to detect the viral proteins. Nuclei were stained with DAPI (blue).

002 on the kinase MEK was assessed using purified recombinant active c-Raf DD, GST-MEK1wt and His-ERK2wt in a cell free reconstitution assay of the Raf/MEK/ERK kinase cascade. Phosphorylation of ERK was measured in an ELISA assay via activation state specific phospho-ERK antibodies and was used as an indication of the activity of the *in vitro* reconstituted Raf/MEK/ERK kinase cascade. For ATR-002, an IC_{50} value of 30.96 nM was measured while an IC_{50} of 2.51 nM was determined for CI-1040 (Fig. 5A, B). Both values are in the low nanomolar range, allowing the conclusion that both, CI-1040 and ATR-002 are very potent MEK inhibiting agents. Nevertheless, the fact that ATR-002 shows a roughly 10-fold higher IC_{50} compared to CI-1040 was in disagreement with published data (Sebolt-Leopold et al., 1999; Tecle et al., 2009). Therefore, we additionally investigated the IC_{50} values of the two compounds in cell-based assays.

A549 and MDCK cells were used to investigate the IC_{50} values in cellular systems. Both cell lines were treated with different concentrations of either CI-1040 or ATR-002. Western blot analysis was performed, and the level of ERK-phosphorylation was investigated using pERK and ERK specific antibodies, and quantified as described in the Materials and methods section (Supplementary S1). Quantification was performed by densitometric analysis. As shown in Fig. 5C the IC_{50} value of CI-1040 for MEK inhibition in A549 cells was 15.5 nM, while the IC_{50} value of ATR-002 was 23-fold higher at 357 nM (Fig. 5C). The IC_{50} of CI-1040 in MDCK cells was 3 nM and 97-fold lower than the IC_{50} of ATR-002, which was 290 nM (Fig. 5D). While the ATR-002 IC_{50} values are similar in A549 cells and MDCK cells, the IC_{50} value of CI-1040 in MDCK cells is 5-fold lower than in A549 cells. For human PBMCs the IC_{50} value of CI-1040 was determined at 4 nM, while it was 15 nM for ATR-002 (Fig. 5E). Here, we also have provided the CC_{50} value of ATR-002 on human PBMCs (Fig. 5F). Based on the IC_{50} values and the use of the GraphPad Prism software 8, we were able to calculate the IC_{90} values for ATR-002 [A549 (3.213 μM), MDCK (2.610 μM), human PBMCs (0.135 μM)] and for CI-1040 [A549 (0.139 μM), MDCK (0.027 μM), human PBMCs (0.036 μM)]. Altogether, these results demonstrated that ATR-002 is a weaker MEK-inhibitor than CI-1040.

3.5. Comparison of ERK-phosphorylation in human PBMCs

Wes (Simple Western™) uses capillary electrophoresis to identify and quantify a protein of interest and the phosphorylation status of a protein. We have used this method to characterize the phosphorylation/activation status of ERK in human PBMCs. Wes (Simple Western™) detects a chemiluminescence signal in the flow-through and calculates the area under the peak, which is then used for quantification. Fig. 6A shows the lane view of the analysis. Detecting a reduced pERK signal demonstrates the inhibitory potential of ATR-002 and CI-1040. The pERK2 intensities were normalized to the loading control (ERK2) by the software. Untreated cells are used as a negative control and PMA/I treated cells show an activated MAPK signaling pathway (positive control). CI-1040 treatment, at a concentration of 10 μM, shows almost a complete inhibition of ERK-phosphorylation. A concentration of 100 μM ATR-002, showed the same inhibition of ERK-phosphorylation as 10 μM CI-1040 (Fig. 6A and B) which agrees with our previous data where we show that roughly 10-fold more ATR-002 is needed to inhibit MEK to the same extent as CI-1040.

3.6. Intracellular uptake

To investigate the reason for the reduced activity of ATR-002 compared to CI-1040, the intracellular uptake of either ATR-002 or CI-1040 was determined. MDCK cells were treated with either 10 μM or 50 μM ATR-002 or CI-1040. At different time points after treatment (0.5, 2, 6 h) cells were harvested, extensively washed and prepared for mass-spectrometry analysis as described in the Materials and methods section. Using a concentration of 10 μM for treatment, an uptake of 73.4 ± 2.6 ng/mL ATR-002 was found (mean of the three time-points). In contrast 7768.8 ± 492.5 ng/mL of intracellular CI-1040 was detected (mean of the three time-points), which is a 105-fold increase compared to ATR-002 (Fig. 6C and D). By using the 50 μM for treatment, an intracellular increase of CI-1040 over time was found and a mean intracellular amount of 32,872.2 ± 596.7 ng/mL (Fig. 6D, grey bars). For 50 μM ATR-002, a mean intracellular uptake of 710.9 ± 61.7 ng/mL was detected (Fig. 6C, grey bars), a 46-fold decrease compared to CI-1040.

3.7. Comparison of plasma concentrations of ATR-002 vs. CI-1040

Next, pharmacokinetics and the bioavailability of ATR-002 and CI-1040 were investigated in a mouse model. NMRI mice were treated via the i.v. or oral route with 150 mg/kg of either CI-1040 or ATR-002.

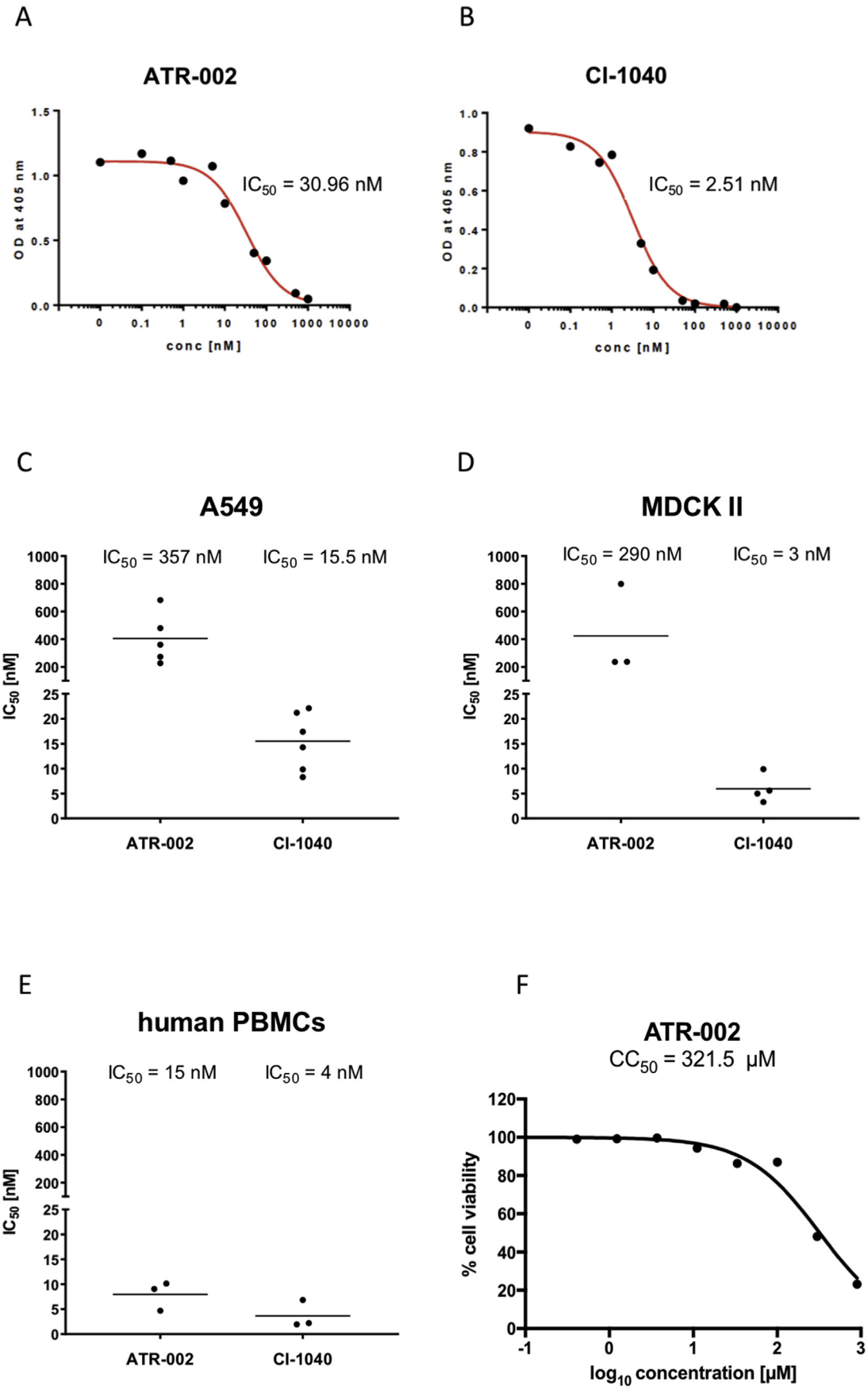

(caption on next page)

Fig. 5. Determination of IC_{50} values for CI-1040 and ATR-002 in cell free kinase assay and IC_{50} values for CI-1040 and ATR-002 in A549, MDCK cells and human PBMCs. (A, B) Cell free kinase assays. As readout, phosphorylated ERK was measured in an ELISA format as described in Materials and methods. **(C)** A549 cells were treated with different concentrations of either CI-1040 or ATR-002 as described in Materials and methods. Six biological replicates were analyzed. IC_{50} for CI-1040 of MEK derived from A549 cells was 15.5 ± 5 nM. IC_{50} for ATR-002 was 357 ± 198 nM. **(D)** For the analysis of MDCK cells treatment was identical to A549 cells. Four biological replicates were analyzed. IC_{50} for CI-1040 of MEK derived from MDCK cells was 3.0 ± 1.1 nM IC_{50} for ATR-002 was 290 ± 168 nM. **(E)** Analyses of human PBMCs were identical to A549 and MDCK cells. Three biological replicates were analyzed. IC_{50} for CI-1040 of MEK derived from PBMCs cells was 4.0 ± 0.8 nM IC_{50} for ATR-002 was 15 ± 1.4 nM. **(F)** CC_{50} value of ATR-002 on human PBMCs.

Blood was collected at different time-points after treatment as indicated in the Materials and methods section. The amount of either ATR-002 or CI-1040 was determined by mass-spectrometry. Pharmacokinetic experiments revealed that after i.v. and oral (Fig. 7A and B, respectively) treatment, larger quantities of ATR-002 (AUC values – i.v.: 860.02 μg*h/ml; oral: 1953.68 μg*h/ml) were found in the plasma of mice compared to CI-1040 (AUC values – i.v.: 223.12 μg*h/ml; oral: 156.16 μg*h/ml). Note that at 8 h post i.v. or post oral application of CI-1040 and 8 h post i.v. application of ATR-002, almost no drug was detectable in the plasma. In contrast, after oral application of ATR-002, a large amount of the drug was detected over the whole time period, which declined only slightly towards the end of the observation period.

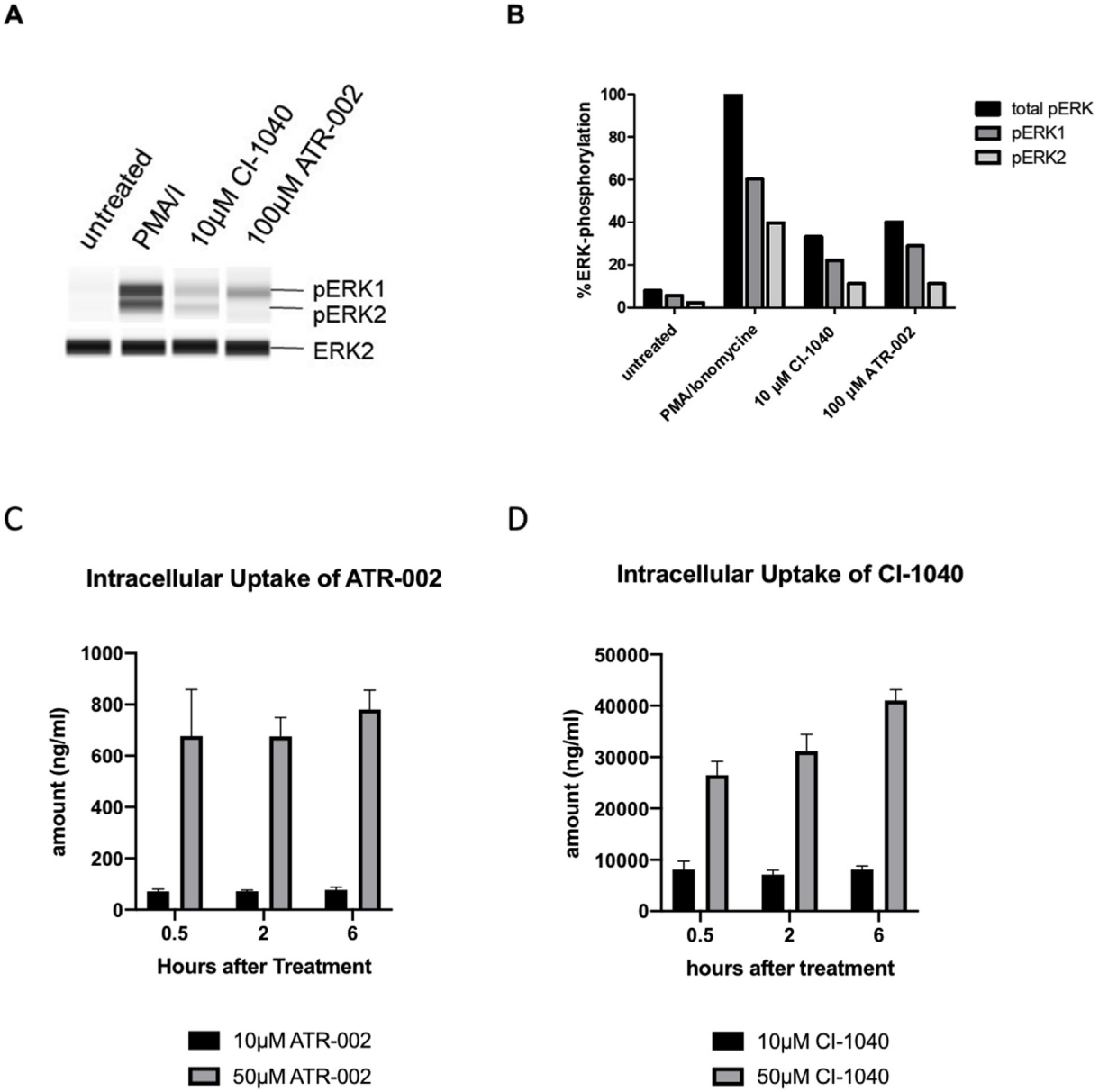

Fig. 6. Comparison of ERK-phosphorylation in human PBMCs and intracellular deposition. Human PBMCs were stimulated with 100 ng/mL PMA und 1 μg/mL Ionomycin (PMA/I) and then treated with 10 μM CI-1040 or 100 μM ATR-002 for 4 h. Untreated cells are used as control. The cells were lysed and then analyzed with Wes technology. **(A)** pERK1/2 and ERK-2 results are shown as gel-like image view. **(B)** Quantification of MEK inhibition with CI-1040 and ATR-002 and comparison of ERK1 (dark grey area) and ERK2 (light grey area) phosphorylation. pERK1/2 were normalized to ERK2 and PMA/I was set as 100%. In all samples ERK1 has increased phosphorylation compared to ERK2. Total ERK (dark grey) was set as 100%, ERK1 and ERK2 was then correlated to this value. **(C, D)** MDCK cells were treated with indicated concentrations of ATR-002 or CI-1040. After extensive washing, cells were harvested, lysed and intracellular deposition was measured using mass spectrometry. 50 to 100-fold more CI-1040 could be detected in MDCKs.

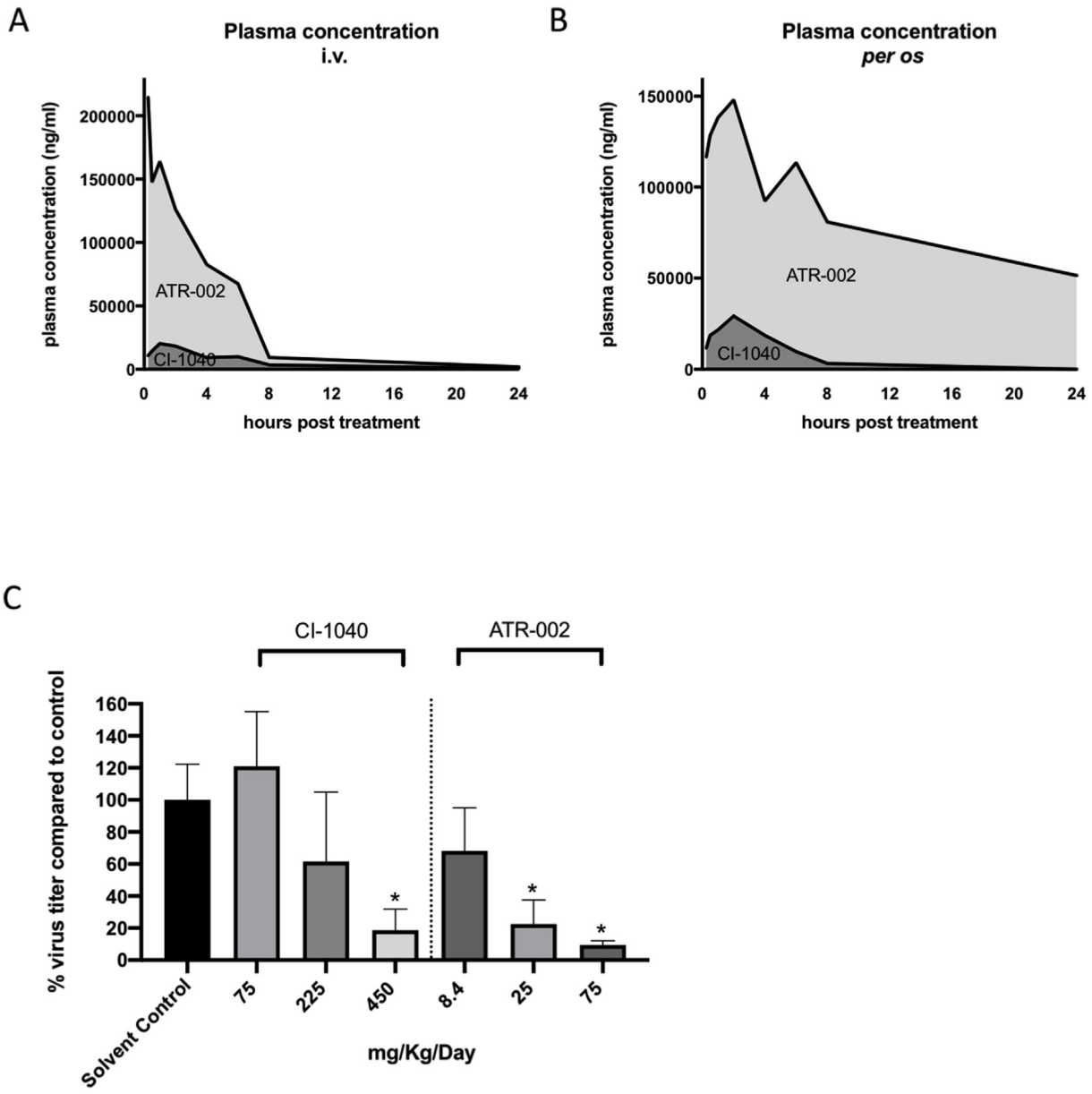

Fig. 7. Comparison of plasma concentration and reduction of virus titer in the lung of mice. Male NMRI mice were either treated with a single dose of either 75 mg/kg CI-1040 (dark grey area) or with 75 mg/kg ATR-002 by the intravenous route **(A)** or with either 150 mg/kg CI-1040 (dark grey area) or with 150 mg/kg ATR-002 using oral gavage **(B)**. Blood was collected at different timepoints after administration and plasma was analyzed for the presence of the drug. Each data point represents the mean value of three plasma samples. GraphPad Prism 7 software was used to illustrate both figures. **(C)** C57BL/6 mice were infected with H1N1pdm09 and treated with different concentrations of either ATR-002 or CI-1040 as indicated. 24 hrs later, mice were sacrificed, lungs were taken and virus titer was determined. Virus titer from solvent treated mice was set as 100% and virus titer reduction compared to solvent control was calculated.

3.8. Reduction of lung virus titers and enhanced survival of CI-1040 and ATR-002-treated mice after lethal H1N1pdm09 infection

In order to determine the actual efficacy of both inhibitors *in vivo* we infected C57BL/6 mice with a lethal dose (3×10^5 pfu) of H1N1pdm09. The mice were treated orally either with a total of 8.4, 25, or 75 mg/kg/day (three times a day (TID) 2.8, 8.4 or 25 mg/kg) ATR-002 or with a total of 25, 225 or 450 mg/kg/day (TID 25, 75 or 150 mg/kg) CI-1040. Twenty-four hours later, the mice were sacrificed, the lungs were taken and the lung virus titer was determined. A significant reduction of virus titer was achieved with a daily dose of 450 mg/kg/day of CI-1040 ($P = 0.0349$; unpaired *t*-test). In contrast, when mice were treated with ATR-002 a daily dose of either 75 mg/kg/Day ($P = 0.0159$; unpaired *t*-test) or 25 mg/kg/Day ($P = 0.0453$; unpaired *t*-test) was sufficient for a significant virus titer reduction (Fig. 7C).

To next investigate the influence of ATR-002 on IAV induced lethality and disease symptoms, when treatment was started at different time points post infection, mice were infected with H1N1pdm09 and treated twice daily orally (9.00 a.m. and 5.00 p.m.) with 25 mg/kg resulting in a total daily dose of 50 mg/kg/day of ATR-002. Treatment started 24, 48 or 72 h post infection. All infected mice developed systemic clinical symptoms. None of the animals died spontaneously because of disease-symptoms. Most of them had to be sacrificed according to animal protection laws due to bodyweight reduction of > 20%. Some of the solvent-treated animals had to be sacrificed because of development of severe disease symptoms in combination with reduction of bodyweight. When treatment started 24 hpi, six out of eight ATR-002-treated mice survived the lethal infection (Fig. 8, blue lines; upper panel).

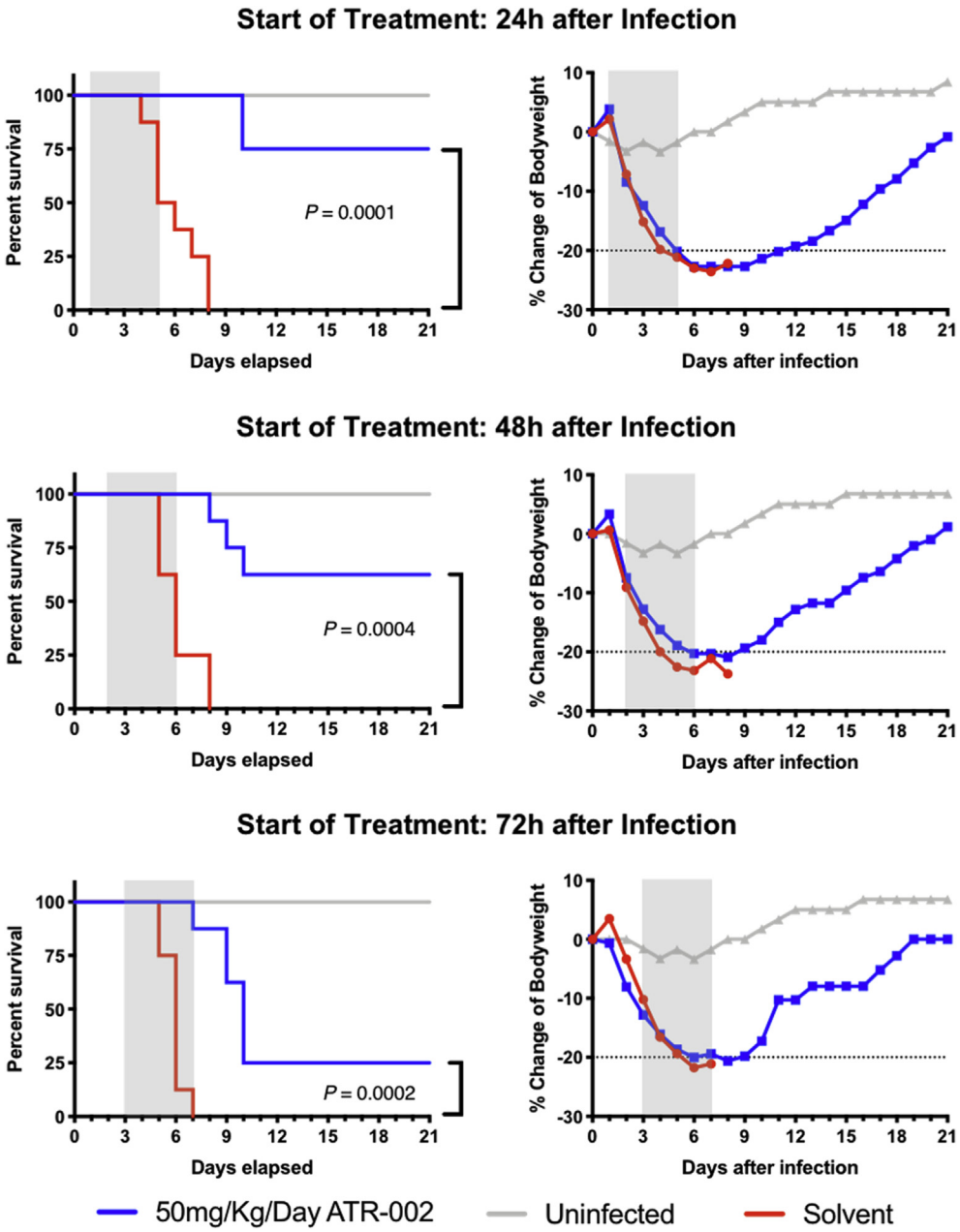

Fig. 8. Survival and bodyweight of IV infected mice treated with ATR-002. Eight female C57BL/6 mice were infected with H1N1pdm09 infection and treated with 50 mg/kg/day (treated twice daily with 25 mg/kg) ATR-002 (blue line) or with solvent alone (red line) via the oral route. Treatment started 24, 48 or 72 hpi for 5 day as indicated in the graphs (grey bar). Mice had to be sacrificed, when a bodyweight reduction of 20% was found (grey dotted line). GraphPad Prism 8 software was used to illustrate both figures. *P*-value was determined using Log-rank (Mantel-Cox) test.

All animals lost weight and developed mild to moderate disease symptoms. Nevertheless, no disease symptoms were observed 14 days post infection and the mice regained bodyweight until the end of the observation period. The difference in survival compared to solvent treated control animals was significant [$P = 0.0001$; Log-rank (Mantel-Cox test)]. When treatment started 48 hpi, three out of eight ATR-002-treated mice (Fig. 8, blue lines; middle panel) survived the lethal infection. Again, all mice lost weight and developed mild to moderate disease symptoms. However, in the surviving animals, no disease symptoms were observed 14 days after infection and the mice regained bodyweight until the end of the observation period. The difference in survival compared to solvent treated control animals was again significant [$P = 0.0004$; Log-rank (Mantel-Cox test)].

When treatment started 72 h after infection, two out of eight ATR-002-treated mice survived the lethal infection (Fig. 8, blue lines; lower panel). All lost weight and developed mild to moderate disease symptoms. Again, the surviving animals showed no disease symptoms and re-gained bodyweight by day 14 after infection. The difference in survival compared to solvent treated control animals was significant [$P = 0.0002$; Log-rank (Mantel-Cox test)]. Three uninfected mice were treated with 50 mg/kg/day ATR-002 for five days. During treatment, they showed a slight reduction of bodyweight (in all animals less than 5%) (Fig. 8, grey lines). After treatment they re-gained bodyweight. These results indicate that ATR-002 treatment started as late as 48 h after infection still influences disease outcomes in mice infected with a lethal H1N1pdm09 dose.

4. Discussion

To date, all licensed influenza drugs and almost all drugs in late

stage clinical development target the virus directly (Koszalka et al., 2017; McKimm-Breschkin et al., 2018; Mifsud et al., 2019). In the past, small molecules have been designed with high specificity against specific viral target protein, such as the neuraminidase, the viral endonuclease and in a more preliminary stage also against the viral nucleoprotein (Ison, 2013; Kao et al., 2010; Koszalka et al., 2017). Even though neuramindase inhibitors are the standard of care to treat influenza, the strategy of targeting the virus directly has an enormous disadvantage, namely the development of virus variants that are less sensitive or even resistant against the respective drug (Cheng et al., 2009; de Jong et al., 2005; Goldhill et al., 2018; Lina et al., 2018; van der Vries et al., 2013). A recent example is Baloxavir, which on one hand demonstrates an impressively fast acting *in vivo* antiviral activity after only one treatment, but on the other hand has already led to the development of resistant virus variants in the course of clinical trial testing (Gubareva et al., 2019; Omoto et al., 2018; Yang, 2019). IV polymerase has no proofreading activity, leading to a high mutation rate and, consequently, to the selection of variants that escape antiviral drugs (Boivin et al., 2010; Drake, 1993). For this reason, it is hypothesized that whenever a drug targets an IV directly, drug resistant variants of the virus will inevitably develop.

The solution to this problem would be to develop either a combinational antiviral therapy, similar to the one available against HIV, or target cellular functions that the virus needs in order to ensure its replication. Approaches using host cell directed targets have already reached clinical stage. DAS181, a recombinant sialidase fusion protein, cleaves the cellular sialic acids, which are required by influenza virus to attach to the host cell (Behzadi and Leyva-Grado, 2019). Nitazoxanide inhibits the trafficking of the HA and thus preventing the assembly of viral particles (Koszalka et al., 2017). We have previously shown that IV needs to activate the Raf/MEK/ERK signaling pathway to survive (Pleschka et al., 2001). By inhibiting this pathway, we were able to demonstrate reduction of virus propagation *in vitro* and *in vivo* (Droebner et al., 2011; Haasbach et al., 2017; Pleschka et al., 2001). Initially, most of our *in vitro* studies were performed with the experimental MEK-inhibitor U0126. While this inhibitor demonstrates excellent MEK-inhibition in cell culture, the bioavailability and stability of this compound *in vivo* is rather weak and the drug does not qualify for further clinical development. Thus, we decided to investigate the MEK-inhibitor, CI-1040, for further *in vivo* studies (Haasbach et al., 2017). Unfortunately, the bioavailability for CI-1040 is also not very high (Lorusso et al., 2005). Moreover, during clinical trial testing, data showed that the active metabolite of CI-1040, PD0184264 (ATR-002) is present in similar higher concentrations in the plasma as the parental compound CI-1040 (Lorusso et al., 2005). Therefore, in the present study we have explored whether ATR-002, similar to CI-1040, would also demonstrate antiviral properties. ATR-002 is the free carboxylate metabolite of CI-1040, lacking the hydroxamic ester part of the parental compound. Based on extensive structure-activity relationships (SAR) findings published for several different MEK-inhibitors (Cheng and Tian, 2017) and the available high-resolution structures of ligand-MEK1/2 complexes (Ohren et al., 2004), it is reasonable to assume that ATR-002 will adopt a binding mode comparable to the vast majority of MEK-inhibitors that are based on the bis-aryl amine chemotype, where Lys-97 might be recognized by the carboxylate moiety of ATR-002. Nevertheless, further investigations need to be performed to finally prove this hypothesis. Interestingly, the kinase exhibits an overall closed conformation similar to the active state of the enzyme, while the activation loop and the helix C within the N-terminal lobe are significantly rearranged compared to the catalytically competent conformation. Additionally, the highly conserved salt bridge between the sidechains of Gln-114 and Lys-97 is disrupted.

We were able to demonstrate antiviral activity of ATR-002 against the seasonal IAV (H1N1pdm09; H3N2) and also against IBV, with EC_{50} values that are higher compared to trametinib, a licensed MEK-inhibitor, but this inhibitor showed a very narrow therapeutic index (Schrader et al., 2018). Interestingly, when compared to the antiviral potential of CI-1040, comparable reduction of virus titer was only achieved with a 10-fold higher concentration of ATR-002 (100 μM vs. 10 μM; Fig. 3). This was unexpected because similar IC_{50} values for CI-1040 and ATR-002 (PD0184264) were previously published. As Tecle and colleagues mentioned, it is difficult to compare the IC_{50} values because of different methods used in separate studies (Tecle et al., 2009). Thus, we have repeated these investigations using a cell free system (Fig. 5A and B), two different cell lines (Fig. 5C and D), and freshly isolated human PBMCs (Fig. 4E). In general, higher IC_{50} values were found in stable cell lines compared to the primary PBMCs. Interestingly, the IC_{50} value for ATR-002 in PBMCs is roughly 2-fold less when compared to the ATR-002 IC_{50} value in the cell free systems (Fig. 5B). This might support the statement that it is difficult to compare different assays for IC_{50} value determination (Tecle et al., 2009). In addition also IC_{90} values were determined, which are in the same range like the EC_{50} value. Regardless of which experimental setup was used, we always found higher IC_{50} values for ATR-002. These findings were also supported by capillary western blot technology (Wes; ProteinSimple®), where we could demonstrate equal inhibition of ERK-phosphorylation, the substrate of MEK, when a 10-fold higher concentration of ATR-002 was used compared to CI-1040. What might be the reason for this apparent difference in IC_{50} values? ATR-002 is a weak acid and these compounds are known to show reduced cell membrane permeability (Saparov et al., 2006). Thus, we investigated, whether this would also be true for ATR-002 by studying the intracellular deposition of ATR-002 in MDCK cells. This cell line was chosen because it represents a very good epithelial model for IAV infection, because it is highly polarized and has high transepithelial electrical resistance (von Bonsdorff et al., 1985). When compared to CI-1040, we found a much lower intracellular deposition for ATR-002 (Fig. 6C and D). This may explain the different IC_{50} values for ATR-002 and CI-1040 in cell lines and primary PBMCs, but it does not explain the different IC_{50} values for the two compounds in the cell free assay (Fig. 5A and B). Nevertheless, from the modeling (Fig. 2) one might speculate a weaker binding affinity of ATR-002 compared to CI-1040.

At this stage of the project it was difficult to see an advantage of ATR-002 over CI-1040. However, the fact that ATR-002 was present in higher amounts in the plasma of patients treated with CI-1040 prompted us to compare the pharmacokinetic properties of CI-1040 and ATR-002 in mice. The higher concentration of ATR-002 (Fig. 7B) might be explained because CI-1040 is metabolized into ATR-002, which reduces the amount of the parental compound in the blood. Indeed, we could detect ATR-002 in CI-1040 treated mice. These results support the observations that ATR-002 is a major active metabolite of CI-1040 and available in higher amounts compared to the parent compound (Lorusso et al., 2005).

Based on these results, we investigated the antiviral potential of ATR-002 against H1N1pdm09 IV infected mice. Due to the high plasma levels of ATR-002 in mice, the amount of ATR-002 that needed to be applied to mice to achieve the same titer reduction was 6-fold lower compared to CI-1040. In our view, these results are fully in line with the pharmacokinetic data. Based on the much better bioavailability of ATR-002 a lower concentration is required for *in vivo* treatment compared to CI-1040. We next questioned whether ATR-002 would also be suitable to protect mice against a lethal H1N1pdm09 infection. For CI-1040 we have already shown that treatment up to 48 hpi is sufficient to protect or partially protect mice against lethal IV infection (Haasbach et al., 2017). In this experiment we started treatment 24, 48 and even 72 h after lethal infection and treated the animals for five consecutive days. Since this represented a multiple dosage treatment scheme, we reduced the daily dosage to 50 mg/kg/day. Based on pharmacokinetic data, ATR-002 was still present in the plasma of mice the next day, when treated with 25 mg/kg twice daily. As shown in Fig. 8, there is no complete protection, but while all of the solvent control animals died, ATR-002 treated animals survived.

In summary, we have demonstrated that ATR-002 has a superior *in vivo* antiviral effect against IV compared to CI-1040. Since treatment of IV infected mice with oseltamivir starting 48 hpi is ineffective, ATR-002 is also superior in this effect. A formal toxicology study in rats and dogs was successful (manuscript in preparation). Therefore, the development of ATR-002 as an antiviral was moved to the next stage. A phase I clinical trial is currently underway.

Acknowledgments

We would like to thank Rebecca Binzberger, Lea Hansen-Palmus, and Magdalena Bauer for their help performing the different IC_{50} assays. This work was supported in part by grants from the Deutsche Forschungsgemeinschaft (Grants Lu477/23-1, SFB1009 B2 and KFO342 to S.L.; SFB 1021 C1 to S.P.), by the German Centre for Infection Research (DZIF), partner site Giessen, Germany (TTU 01.803 Broad-spectrum Antivirals to S.P.). S.L. O.P. and S.P. are members of the German FluResearchNet, a nationwide research network on zoonotic influenza.

Appendix A. Supplementary data

Supplementary data to this article can be found online at https://doi.org/10.1016/j.antiviral.2020.104806.

References

Baranovich, T., Saito, R., Suzuki, Y., Zaraket, H., Dapat, C., Caperig-Dapat, I., Oguma, T., Shabana, I.I., Saito, T., Suzuki, H., Japanese Influenza Collaborative Study, G, 2010. Emergence of H274Y oseltamivir-resistant A(H1N1) influenza viruses in Japan during the 2008-2009 season. J. Clin. Virol. 47, 23–28.

Behzadi, M.A., Leyva-Grado, V.H., 2019. Overview of current therapeutics and novel candidates against influenza, respiratory syncytial virus, and Middle East respiratory syndrome coronavirus infections. Front. Microbiol. 10, 1327.

Belshe, R.B., Edwards, K.M., Vesikari, T., Black, S.V., Walker, R.E., Hultquist, M., Kemble, G., Connor, E.M., Group, C.-T.C.E.S., 2007. Live attenuated versus inactivated influenza vaccine in infants and young children. N. Engl. J. Med. 356, 685–696.

Boivin, S., Cusack, S., Ruigrok, R.W., Hart, D.J., 2010. Influenza A virus polymerase: structural insights into replication and host adaptation mechanisms. J. Biol. Chem. 285, 28411–28417.

Cheng, P.K., Leung, T.W., Ho, E.C., Leung, P.C., Ng, A.Y., Lai, M.Y., Lim, W.W., 2009. Oseltamivir- and amantadine-resistant influenza viruses A (H1N1). Emerg. Infect. Dis. 15, 966–968.

Cheng, Y., Tian, H., 2017. Current development status of MEK inhibitors. Molecules 22, 1–20.

Correia, V., Santos, L.A., Giria, M., Almeida-Santos, M.M., Rebelo-de-Andrade, H., 2015. Influenza A(H1N1)pdm09 resistance and cross-decreased susceptibility to oseltamivir and zanamivir antiviral drugs. J. Med. Virol. 87, 45–56.

de Jong, M.D., Tran, T.T., Truong, H.K., Vo, M.H., Smith, G.J., Nguyen, V.C., Bach, V.C., Phan, T.Q., Do, Q.H., Guan, Y., Peiris, J.S., Tran, T.H., Farrar, J., 2005. Oseltamivir resistance during treatment of influenza A (H5N1) infection. N. Engl. J. Med. 353, 2667–2672.

Dong, G., Peng, C., Luo, J., Wang, C., Han, L., Wu, B., Ji, G., He, H., 2015. Adamantane-resistant influenza a viruses in the world (1902-2013): frequency and distribution of M2 gene mutations. PloS One 10, e0119115.

Drake, J.W., 1993. Rates of spontaneous mutation among RNA viruses. Proc. Natl. Acad. Sci. U. S. A. 90, 4171–4175.

Droebner, K., Pleschka, S., Ludwig, S., Planz, O., 2011. Antiviral activity of the MEK-inhibitor U0126 against pandemic H1N1v and highly pathogenic avian influenza virus in vitro and in vivo. Antivir. Res. 92, 195–203.

Goldhill, D.H., Te Velthuis, A.J.W., Fletcher, R.A., Langat, P., Zambon, M., Lackenby, A., Barclay, W.S., 2018. The mechanism of resistance to favipiravir in influenza. Proc. Natl. Acad. Sci. U. S. A. 115, 11613–11618.

Gubareva, L.V., Mishin, V.P., Patel, M.C., Chesnokov, A., Nguyen, H.T., De La Cruz, J., Spencer, S., Campbell, A.P., Sinner, M., Reid, H., Garten, R., Katz, J.M., Fry, A.M., Barnes, J., Wentworth, D.E., 2019. Assessing baloxavir susceptibility of influenza viruses circulating in the United States during the 2016/17 and 2017/18 seasons. Euro Surveill. 24, 1–5.

Haasbach, E., Muller, C., Ehrhardt, C., Schreiber, A., Pleschka, S., Ludwig, S., Planz, O., 2017. The MEK-inhibitor CI-1040 displays a broad anti-influenza virus activity in vitro and provides a prolonged treatment window compared to standard of care in vivo. Antivir. Res. 142, 178–184.

Haasbach, E., Pauli, E.K., Spranger, R., Mitzner, D., Schubert, U., Kircheis, R., Planz, O., 2011. Antiviral activity of the proteasome inhibitor VL-01 against influenza A viruses. Antivir. Res. 91, 304–313.

Ison, M.G., 2013. Clinical use of approved influenza antivirals: therapy and prophylaxis. Influenza Other Respir Viruses 7 (Suppl. 1), 7–13.

Iuliano, A.D., Roguski, K.M., Chang, H.H., Muscatello, D.J., Palekar, R., Tempia, S., Cohen, C., Gran, J.M., Schanzer, D., Cowling, B.J., Wu, P., Kyncl, J., Ang, L.W., Park, M., Redlberger-Fritz, M., Yu, H., Espenhain, L., Krishnan, A., Emukule, G., van Asten, L., Pereira da Silva, S., Aungkulanon, S., Buchholz, U., Widdowson, M.A., Bresee, J.S., Global Seasonal Influenza-associated Mortality Collaborator, N, 2018. Estimates of global seasonal influenza-associated respiratory mortality: a modelling study. Lancet 391, 1285–1300.

Kao, R.Y., Yang, D., Lau, L.S., Tsui, W.H., Hu, L., Dai, J., Chan, M.P., Chan, C.M., Wang, P., Zheng, B.J., Sun, J., Huang, J.D., Madar, J., Chen, G., Chen, H., Guan, Y., Yuen, K.Y., 2010. Identification of influenza A nucleoprotein as an antiviral target. Nat. Biotechnol. 28, 600–605.

Kiso, M., Mitamura, K., Sakai-Tagawa, Y., Shiraishi, K., Kawakami, C., Kimura, K., Hayden, F.G., Sugaya, N., Kawaoka, Y., 2004. Resistant influenza A viruses in children treated with oseltamivir: descriptive study. Lancet 364, 759–765.

Koszalka, P., Tilmanis, D., Hurt, A.C., 2017. Influenza antivirals currently in late-phase clinical trial. Influenza Other Respir Viruses 11, 240–246.

Lambert, L.C., Fauci, A.S., 2010. Influenza vaccines for the future. N. Engl. J. Med. 363, 2036–2044.

Lina, B., Boucher, C., Osterhaus, A., Monto, A.S., Schutten, M., Whitley, R.J., Nguyen-Van-Tam, J.S., 2018. Five years of monitoring for the emergence of oseltamivir resistance in patients with influenza A infections in the Influenza Resistance Information Study. Influenza Other Respir Viruses 12, 267–278.

Lorusso, P.M., Adjei, A.A., Varterasian, M., Gadgeel, S., Reid, J., Mitchell, D.Y., Hanson, L., DeLuca, P., Bruzek, L., Piens, J., Asbury, P., Van Becelaere, K., Herrera, R., Sebolt-Leopold, J., Meyer, M.B., 2005. Phase I and pharmacodynamic study of the oral MEK inhibitor CI-1040 in patients with advanced malignancies. J. Clin. Oncol. 23, 5281–5293.

Ludwig, S., Pleschka, S., Planz, O., Wolff, T., 2006. Ringing the alarm bells: signalling and apoptosis in influenza virus infected cells. Cell Microbiol. 8, 375–386.

Ludwig, S., Wolff, T., Ehrhardt, C., Wurzer, W.J., Reinhardt, J., Planz, O., Pleschka, S., 2004. MEK inhibition impairs influenza B virus propagation without emergence of resistant variants. FEBS Lett. 561, 37–43.

Matrosovich, M., Matrosovich, T., Garten, W., Klenk, H.D., 2006. New low-viscosity overlay medium for viral plaque assays. Virol. J. 3, 63.

McKimm-Breschkin, J.L., Jiang, S.B., Hui, D.S., Beigel, J.H., Govorkova, E.A., Lee, N., 2018. Prevention and treatment of respiratory viral infections: presentations on antivirals, traditional therapies and host-directed interventions at the 5th ISIRV Antiviral Group conference. Antivir. Res. 149, 118–142.

Mifsud, E.J., Hayden, F.G., Hurt, A.C., 2019. Antivirals targeting the polymerase complex of influenza viruses. Antivir. Res. 169, 104545.

Nichol, K.L., Lind, A., Margolis, K.L., Murdoch, M., McFadden, R., Hauge, M., Magnan, S., Drake, M., 1995. The effectiveness of vaccination against influenza in healthy, working adults. N. Engl. J. Med. 333, 889–893.

Nichol, K.L., Treanor, J.J., 2006. Vaccines for seasonal and pandemic influenza. J. Infect. Dis. 194 (Suppl. 2), S111–S118.

Ohren, J.F., Chen, H., Pavlovsky, A., Whitehead, C., Zhang, E., Kuffa, P., Yan, C., McConnell, P., Spessard, C., Banotai, C., Mueller, W.T., Delaney, A., Omer, C., Sebolt-Leopold, J., Dudley, D.T., Leung, I.K., Flamme, C., Warmus, J., Kaufman, M., Barrett, S., Tecle, H., Hasemann, C.A., 2004. Structures of human MAP kinase kinase 1 (MEK1) and MEK2 describe novel noncompetitive kinase inhibition. Nat. Struct. Mol. Biol. 11, 1192–1197.

Olschlager, V., Pleschka, S., Fischer, T., Rziha, H.J., Wurzer, W., Stitz, L., Rapp, U.R., Ludwig, S., Planz, O., 2004. Lung-specific expression of active Raf kinase results in increased mortality of influenza A virus-infected mice. Oncogene 23, 6639–6646.

Omoto, S., Speranzini, V., Hashimoto, T., Noshi, T., Yamaguchi, H., Kawai, M., Kawaguchi, K., Uehara, T., Shishido, T., Naito, A., Cusack, S., 2018. Characterization of influenza virus variants induced by treatment with the endonuclease inhibitor baloxavir marboxil. Sci. Rep. 8, 9633.

Planz, O., 2013. Development of cellular signaling pathway inhibitors as new antivirals against influenza. Antivir. Res. 98, 457–468.

Pleschka, S., Wolff, T., Ehrhardt, C., Hobom, G., Planz, O., Rapp, U.R., Ludwig, S., 2001. Influenza virus propagation is impaired by inhibition of the Raf/MEK/ERK signalling cascade. Nat. Cell Biol. 3, 301–305.

Putri, W., Muscatello, D.J., Stockwell, M.S., Newall, A.T., 2018. Economic burden of seasonal influenza in the United States. Vaccine 36, 3960–3966.

Radin, J.M., Hawksworth, A.W., Myers, C.A., Ricketts, M.N., Hansen, E.A., Brice, G.T., 2016. Influenza vaccine effectiveness: maintained protection throughout the duration of influenza seasons 2010-2011 through 2013-2014. Vaccine 34, 3907–3912.

Saparov, S.M., Antonenko, Y.N., Pohl, P., 2006. A new model of weak acid permeation through membranes revisited: does Overton still rule? Biophys. J. 90, L86–L88.

Schrader, T., Dudek, S.E., Schreiber, A., Ehrhardt, C., Planz, O., Ludwig, S., 2018. The clinically approved MEK inhibitor Trametinib efficiently blocks influenza A virus propagation and cytokine expression. Antivir. Res. 157, 80–92.

Sebolt-Leopold, J.S., 2004. MEK inhibitors: a therapeutic approach to targeting the Ras-MAP kinase pathway in tumors. Curr. Pharmaceut. Des. 10, 1907–1914.

Sebolt-Leopold, J.S., Dudley, D.T., Herrera, R., Van Becelaere, K., Wiland, A., Gowan, R.C., Tecle, H., Barrett, S.D., Bridges, A., Przybranowski, S., Leopold, W.R., Saltiel, A.R., 1999. Blockade of the MAP kinase pathway suppresses growth of colon tumors in vivo. Nat. Med. 5, 810–816.

Tecle, H., Shao, J.X., Li, Y.H., Kothe, M., Kazmirski, S., Penzotti, J., Ding, Y.H., Ohren, J., Moshinsky, D., Coli, R., Jhawar, N., Bora, E., Jacques-O'Hagan, S., Wua, J., 2009. Beyond the MEK-pocket: can current MEK kinase inhibitors be utilized to synthesize novel type III NCKIs? Does the MEK-pocket exist in kinases other than MEK? Bioorg. Med. Chem. Lett 19, 226–229.

Tempia, S., Moyes, J., Cohen, A.L., Walaza, S., Edoka, I., McMorrow, M.L., Treurnicht, F.K., Hellferscee, O., Wolter, N., von Gottberg, A., Nguweneza, A., McAnerney, J.M.,

Dawood, H., Variava, E., Cohen, C., 2019. Health and economic burden of influenza-associated illness in South Africa, 2013-2015. Influenza Other Respir Viruses 484–495.
van der Vries, E., Schutten, M., Fraaij, P., Boucher, C., Osterhaus, A., 2013. Influenza virus resistance to antiviral therapy. Adv. Pharmacol. 67, 217–246.
von Bonsdorff, C.H., Fuller, S.D., Simons, K., 1985. Apical and basolateral endocytosis in Madin-Darby canine kidney (MDCK) cells grown on nitrocellulose filters. EMBO J. 4, 2781–2792.
Yang, T., 2019. Baloxavir marboxil: the first cap-dependent endonuclease inhibitor for the treatment of influenza. Ann. Pharmacother. 53, 754–759.